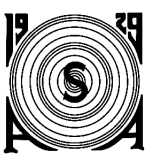

euronoise

The fast wave propagation in bovine cancellous bone -experiments and simulation

Mami Matsukawa[a], Katsunori Mizuno[a] and Yoshiki Nagatani[b]

[a]Doshisha University, 1-3, Tatara Miyakodani, 610-0321 Kyotanabe, Japan
[b]Nara Medical University, 840 Shijo-cho, 634-8522 Kashihara, Japan
mmatsuka@mail.doshisha.ac.jp

In the cancellous bone, two types of longitudinal waves, fast and slow waves, are observed when the waves propagate parallel to the trabeculae direction. Paying special attention to the wave front of observed waves, we have experimentally made clear the effect of anisotropy on the fast wave speed. We have also compared the experimental results of fast waves with the simulation studies, using the three dimensional X-ray CT data and the Finite-Difference Time-Domain (FDTD) method. In spite of the lack of attenuation effects in the simulation, we can find interesting similarity between the fast wave speeds obtained by experiments and simulation. In addition, the characteristic attenuation behaviours of fast wave were found in both experiments and simulations. Attenuation of fast wave is always higher in the early state of propagation.

1. Introduction

Quantitative ultrasound (QUS) has become an important technique to assess the status of bone [1]. QUS parameters are closely related to the structural properties and elastic properties [2-4], which cannot be obtained by X-ray measurements or other nondestructive techniques. This is because these other techniques usually measure the amount of bone, for example, the mineral content.

Despite the increasing use of this QUS technique, it is still difficult to obtain precise information about bones. One attempt for the precise evaluation is the measurement of cancellous bone, which is a good indicator of osteoporosis [5]. However, cancellous bone is anisotropic, heterogeneous, and composed of a complicated network structure called trabeculae in the soft tissue (bone marrow), which result in the complicated wave propagation phenomena. Many experimental and theoretical studies have been reported on the interactions between ultrasound waves and the cancellous structure. Hosokawa and Otani have reported the characteristic wave propagation and experimentally made clear the separation of longitudinal waves into fast and slow waves [6-7]. The introduction of this two-wave phenomenon increased the QUS parameters and brought us more information of the cancellous structure.

On the other hand, another recent approach to understand the wave propagation is the direct analysis of wave equation. If the 3-D numerical simulation of wave propagation on bone is successfully performed, it shall give us the visual image of complicated wave propagation. Therefore, from the approach by Luo et al., several studies have reported the simulation of complicated wave propagation in cancellous bone [8]. Using a 3-D synchrotron micro tomography of actual trabeculae, Bossy et al. [9], Padilla et al. [10] and Haiat et al. [11] have reported the generation of fast and slow waves using finite-difference time-domain (FDTD) simulation. We have also tried to introduce the elastic FDTD method for the simulation of two wave propagation in cancellous bone, using three-dimensional X-ray CT images [12,13]. Since the simulation easily enables the visualization of various wave propagations, it is very useful not only for understanding the behavior of sound wave but also for an optimal design of a new diagnostic system.

In this study, therefore, we would like to discuss the wave propagation in the cancellous bone, from both experimental and simulation approaches. Here, we pay special attention to the fast wave propagation, because the fast wave mainly propagates in trabeculae and reflects its structure. Making use of the cancellous bone information obtained by X-ray micro-computed tomography (CT), the fast wave propagation is investigated considering the anisotropy in speeds and attenuation characteristics.

2. Sample preparation

In the following specimen preparation, the cancellous bones in the distal part of bovine femora were used. All specimens were defatted by boiling. To remove air bubbles trapped in the cancellous bone, the specimens were degassed in water for 60 min before the ultrasonic measurements.

2.1. Cylindrical specimen for anisotropy measurements

Specimens were obtained from 30 month-old bovine left femur. The cancellous bone in the distal part was removed and made into rectangular samples. Because most *in vivo* clinical techniques uses the ultrasonic waves propagating perpendicular to the bone axis, we took these rectangular samples along the bone axis (Fig.1). The cylindrical specimens, which were about 40–70 mm in length and 11.00±0.05 mm in diameter, were formed from these rectangular samples.

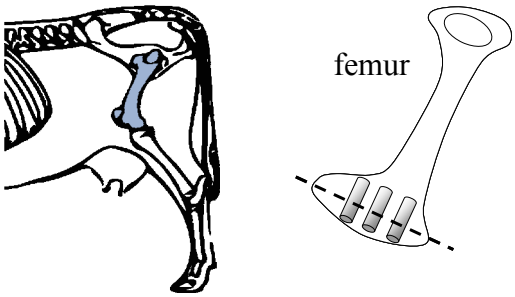

Fig.1 Cylindrical specimen.

2.2. Rectangular specimen for attenuation measurements

Specimens were obtained from 36 month-old bovine left femur. The cancellous bone in the distal part was removed and made into rectangular specimens. The size of bone specimens were 20×20×15 mm. In these specimens, the wave always propagates in the direction of bone axis. Several measurements were performed using a specimen by changing the specimen thickness.

3. Experiments

In the following two experiments, the same experimental system is used except for the transducer type and geometry of transducer and specimens. In common, a function generator (33250A; Agilent Technologies) delivered electrical pulses to the transmitter. A single sinusoidal signal of 1 MHz, 50 Vp-p was applied to the transmitter. The longitudinal wave propagated through water, sample, and water. The other transducer received the wave and converted it into an electrical signal. The signal was amplified by a 40-dB preamplifier (5307; NF) and visualized with an oscilloscope (TDS524A; Tektronix).

CT images of the specimens were obtained using X-ray micro-CT (MCT-12505MF; Hitachi, or SMX100-CT Shimadzu). Here, the defatted specimens were scanned in air.

3.1. Experiments for Anisotropy measurements

A PVDF focus transmitter 20 mm in diameter with a focal length of 40 mm (Custom made; Toray, Yokohama, Japan) and a self-made PVDF receiver 10 mm in diameter were used in this experiment. Both PVDF transducers were mounted coaxially with a distance of 60 mm in degassed water at room temperature. We placed the focal point of sound on the central axis of the cylindrical specimen as shown in Fig.2. The direction of the incident wave was always perpendicular to the side surface of the cylindrical specimen. The measurements were performed by changing the position along the cylindrical axis and the incident angle.

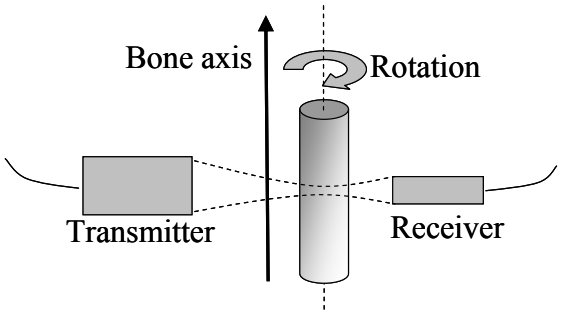

Fig.2 Anisotropic wave speed measurements using cylindrical specimen.

3.2. Experiments for attenuation measurements

The bone specimen and plane square PVDF transducers were immersed in degassed water in an acoustical tube at room temperature. The surface area of the plane PVDF transmitter and receiver (self-made, PVDF films used) were 20×20 mm. This comparatively large transducer brings good signal to noise ratio of the observed waves. The distance between two transducers was 60 mm. A rectangular specimen was mounted between the transducers.

4. Simulation of wave propagation

4.1. FDTD method

We have used the governing equations of 3 dimensional elastic FDTD method for the isotropic medium. For example, the empirical equations for the *x* direction are shown here.

$$\frac{\partial \sigma_{xx}}{\partial t} = (\lambda + 2\mu)\frac{\partial v_x}{\partial x} + \lambda \frac{\partial v_y}{\partial y} + \lambda \frac{\partial v_z}{\partial z}, \quad (1)$$

$$\frac{\partial \sigma_{xy}}{\partial t} = \mu\left(\frac{\partial v_x}{\partial y} + \frac{\partial v_y}{\partial x}\right), \quad (2)$$

$$\frac{\partial v_x}{\partial t} = \frac{1}{\rho}\left(\frac{\partial \sigma_{xx}}{\partial x} + \frac{\partial \sigma_{xy}}{\partial y} + \frac{\partial \sigma_{zx}}{\partial z}\right), \quad (3)$$

Here, σ_{ij} is the normal and shear stresses, v_i is particle velocity, λ and μ are Lame's coefficients, ρ is density of the medium. In this simulation, the elastic anisotropy in the solid part (trabeculae) and attenuation was not considered. Using the same equations for y and z directions, the stress and particle velocity were calculated alternately both in the spatial and time domains. The FDTD simulation software was originally programmed by our group [13].

4.2. Simulating procedure

For the simulation of cylindrical specimen, we have used the whole CT data. The total simulation field was 13 × 15 × 17 mm with cube lattice of 47.5 μm. Time step for simulation was 5 ns. By rotating the 3 dimensional specimen data in the simulation field, we have obtained the waves which passed through the specimen. Because of the memory problem, we have assumed the transmitter with diameter of 9.5 mm, which is smaller than that used in the experiments.

For the simulation to investigate attenuation, the size of specimens used was 15 by 15mm and 9-12 mm in thickness. Because of the memory problem, we used the centre part of specimen CT data. **Figure 3** is an example of X-ray micro focus CT images. Spatial resolution of the CT images was 47.5 μm.

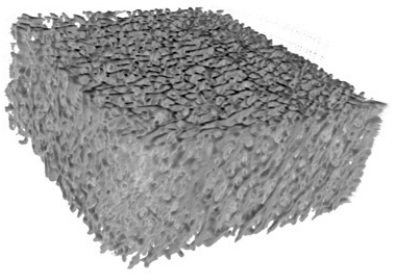

Fig.3 An example of CT images of rectangular specimen. 3-D reconstruction was made by 3D-bon software (Ratoc).

The total simulation field was 21 × 21× 18 mm with cube lattice of 57 μm. Time step for simulation was 4 ns.

In these simulations, as the initial waveform at the surface of the plane source transducer, we used the experimentally observed waveform of a single sinusoidal sound wave at 1 MHz that passed through the water. For the material parameters for both simulations, we used the reported longitudinal wave speed and density in the bovine cortical bone [15] and Poisson's ratio of 0.34.

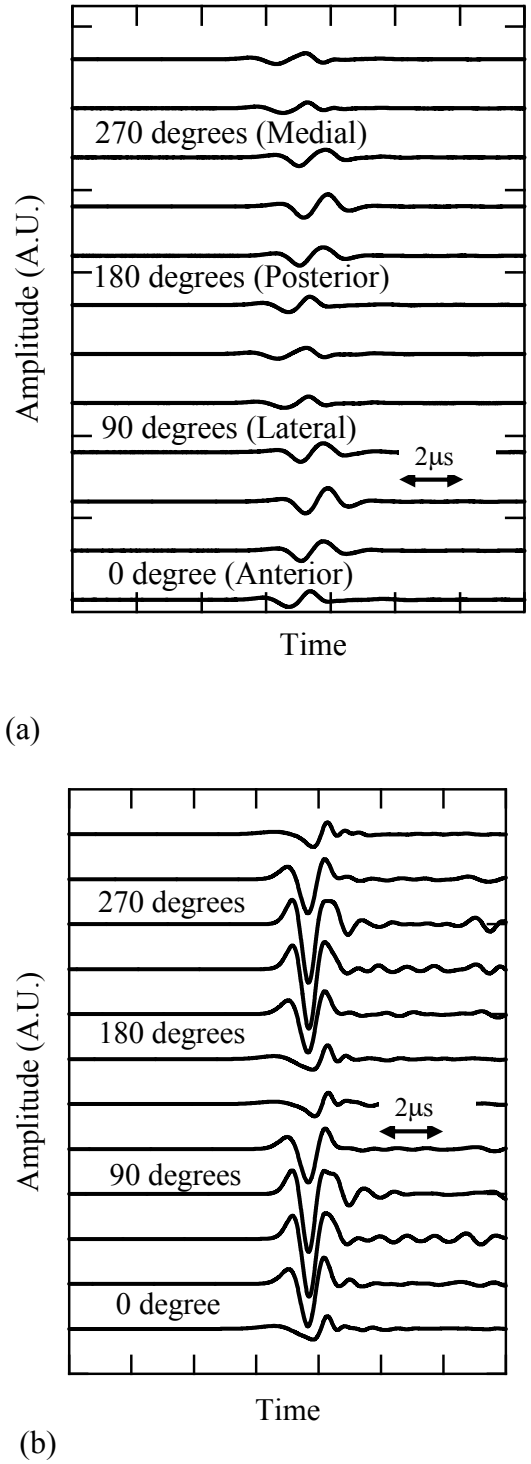

Fig.4 Changes in observed waveform as a function of incident angle to a cylindrical specimen. The degree in the figure indicates the rotation angle. (a) experiments, (b) simulation.

5. Results and discussion

5.1. Anisotropy of the fast wave speed

Figure 4 shows an example of the periodic changes in the fast wave observed from a cylindrical specimen. The wave fronts in Fig.4 are always observed faster than that of the wave which passed through water only. This tells us the existence of fast wave although the clear separation of fast and slow wave cannot be observed. Therefore, focusing on the position of the wave front, we can find that the fast wave speeds clearly depended on the incident angle. In this specimen, the fast wave speed showed a maximum value when the ultrasonic waves propagated from the anterior medial part to the posterior lateral part or *vice versa*. This direction corresponded to the predominant orientation of the trabeculae. The difference between the maximum and minimum speed values was dependent on the positions of the specimens, showing the distribution of anisotropy. Figure 4 shows similar tendency between experimental and simulation results. The amplitude changes due to the angle are dramatic in simulation, which seems to result from the lack of attenuation factor.

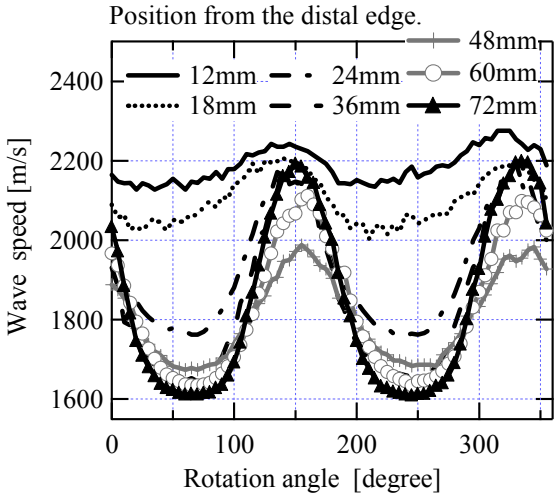

Fig.5 Periodic changes of the fast wave speed as a function of position from the distal edge in the cylindrical specimen. Experimental.

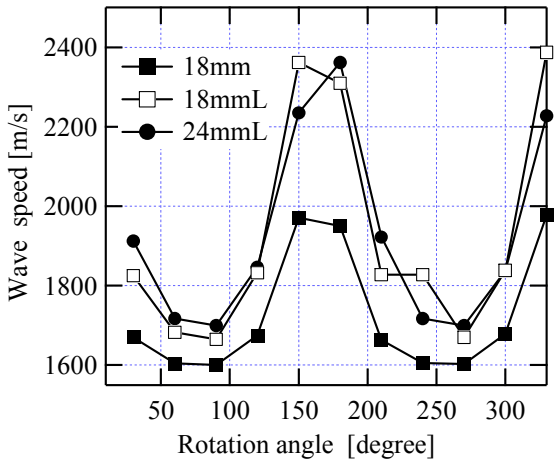

Fig.6 Periodic changes of the fast wave speed. 18mmL and 24mmL mean the comparatively large trabeculae models. Simulation.

Figure 5 shows the periodic speed changes due to the position in the cylindrical specimen. We have changed the measurement position by moving the specimen in the direction of an arrow in Fig.2. The dynamic changes in wave speed tell that the anisotropy becomes strong with the distance from the distal edge. Another interesting result is the averaged wave speed of all angle data at each position. Near the distal edge, the averaged speed is comparatively high. We have already reported that the dynamic speed changes indicate the degree of anisotropy whereas the averaged speed in one position depends on the bone volume fraction (BV/TV). [14] Our present data tells us the comparatively high BV/TV in the distal edge.

Figure 6 gives the anisotropy results of simulated wave speed. We can find the similar anisotropic tendency of speed, however, the maximum and minimum values are different. In addition to the lack of attenuation factor in the medium, one reason seems to be the binarizing problem. We have tried to simulate using two trabeculae models of the same bone. In case of comparatively thick trabeculae model, the anisotropy becomes strong. This tells the difficulty for obtaining models from CT data, which usually includes some ambiguity in the images. One should also note here the slight difference of simulation models from the actual bone. Due to the restriction of memory, we could not assume the actual transmitter model, which was used in the experiments. The assumption of smaller transmitter causes the comparatively large focal area, which also seems to result in the differences between the experiments and simulation.

5.2. Attenuation of the fast wave

Next, attenuation of the fast wave was investigated from both experimental and simulation approaches. Figure 6 shows a typical experimental waveform (thickness 8.45mm). We can see small amplitudes of the fast waves were always much smaller than those of the slow waves, which has also been observed in the simulated waveforms [13]. We then obtained the distribution of fast wave attenuation by decreasing the thickness of the specimen. Actually, in both simulation and experiments, we deleted each 1mm slice and simulated or measured the waveform. From the peak amplitudes of fast waves obtained at each thickness, the distribution of attenuation [dB/mm] can be evaluated; e.g. using peak amplitudes obtained from 10 mm and 9 mm thick specimens, we obtained the distribution of attenuation values between the positions from 9 to 10 mm from the surface.

The distribution of BV/TV (bone volume / total volume) and fast wave attenuation is shown in **Figs. 7**. Because the longitudinal wave always enters the sample from the position 0, this result tells that the fast wave attenuation is higher in the early state of propagation. In addition, the attenuation values are similar.

One reason for this interesting attenuation phenomenon is considered to come from the complicated propagation path of longitudinal waves. The fast wave mainly propagates in the trabeculae of cancellous bone. Alignment of trabeculae is not always parallel to the propagation direction. Figures 8

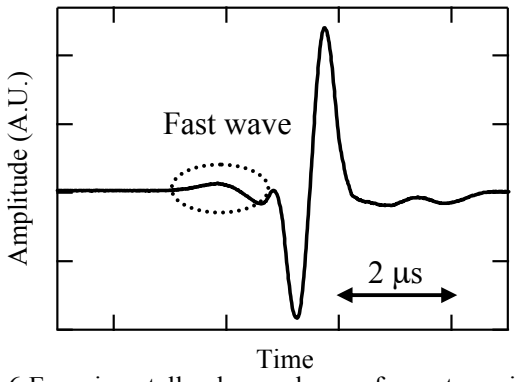

Fig.6 Experimentally observed wave form at specimen thickness of 9mm.

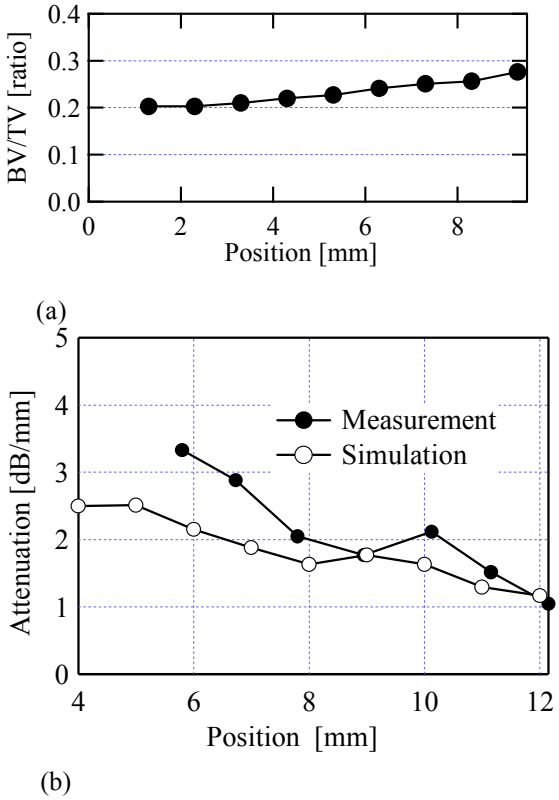

Fig.7 Distribution of BV/TV and fast wave attenuation in a typical sample.

show examples of the wave propagation. The bone model is shown in Fig. 8 (a). The black structure indicates solid part (trabeculae). For comparison, Fig.8 (b) shows the distribution of wave in water. We can see clear wave front. Figure 8 (c) is the result of the bone model. Due to the various paths of trabeculae, the wave front of fast wave is not uniform in the early state of propagation. This irregularity of wave front then seems to cause the apparent higher attenuation of fast wave. These results tell us that the fast wave requires certain propagation distance to form in-phase wave front and steady attenuation. This also means that the fast wave attenuation is difficult to be used as an indicator of the structural properties of cancellous bone for the characterization of thin cancellous bone samples.

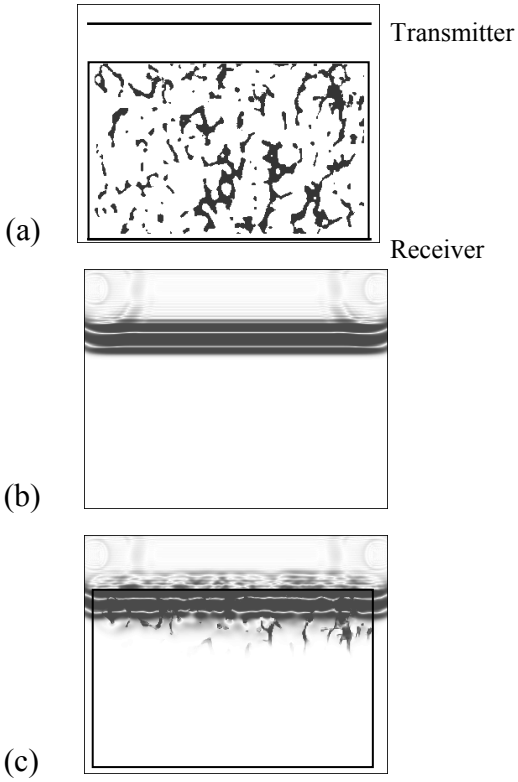

Fig.8 Simulated wave propagation in a typical specimen. (a) simulated area, (b) wave propagation in water, (c) wave propagation in the early state (2.5μs).

6. Conclusion

Experimental and simulation investigation of fast wave propagation was discussed. The FDTD simulation results showed similar tendency in the evaluation of anisotropy and attenuation. Especially, the visualization of propagation phenomena gives us important information to understand the complicated wave propagation process in trabecular bone.

Acknowledgments

Authors would like to show special thanks to Mr. Saeki and Mr. Soumiya for their support during experiments.

This study was partly supported by a bilateral joint project between JSPS and CNRS, the Academic Research Frontier project of Doshisha University and Ministry of Education, Culture, Sports, Science and Technology, in addition to the Grants–in–Aid for Scientific research (B) supported by Japan Society for the Promotion of Science.

References

[1] C. F. Njeh. “Quantitative ultrasound: assessment of osteoporosis and bone status’, 1st ed. 1999 (Taylor & Francis)

[2] R. Barkmann, E. Kantorovich, C. Singal, D. Hans, H. Genant, M. Heller and C. Glüer. “A new method for quantitative ultrasound measurements at multiple skeletal sites.” *J Clin Densitometry,* 3, 1–7 (2000)

[3] M. L. Bouxsein and S. E. Radloff. “Quantitative ultrasound of the calcaneus reflects the mechanical properties of calcaneal trabecular bone.” *J Bone Miner. Res.,* vol. 12, pp. 839–846 (1997)

[4] C. F. Njeh, C. W. Kuo, C. M. Langton, H. I. Atrah and C. M. Boivin. “Prediction of human femoral bone strength using ultrasound speed and BMD: an in vitro study.” *Osteoporosis Int.*, 7, 471–477 (1997)

[5] J. K. Weaver and S. J. Chalmer. “Cancellous bone: its strength and changes with aging and an evaluation of some methods for measuring mineral content 1. Aging changes in cancellous bone.” *J. Bone Joint Surg.,* 48, 289–298 (1996)

[6] A. Hosokawa and T. Otani. “Ultrasonic wave propagation in bovine cancellous bone.” *J. Acous. Soc. Am.*, 101, 558–562 (1997)

[7] A. Hosokawa and T. Otani. “Acoustic anisotropy in bovine cancellous bone.” *J. Acous. Soc. Am.,* 103, 2718–2722 (1998)

[8] G. Luo, J. J. Kaufman, A. Chiabrera, B. Bianco, J. H. Kinney, D. Haupt, J. T. Ryaby and R. S. Siffert: "Computational methods for ultrasonic bone assessment," *Ultrasound in Med. & Biol.,* 25, 823-830 (1999)

[9] E. Bossy, F. Padilla, F. Peyrin and P. Laugier : "Three-dimensional simulation of ultrasound propagation through trabecular bone structures measured by synchrotron microtomography," *Phys. Med. Biol.* 50 5545-5556 (2005)

[10] F. Padilla, E. Bossy and P. Laugier: "Simulation of Ultrasound Propagation Through Three-Dimensional Trabecular Bone Structures: Comparison with Experimental Data," *Jpn. J. Appl. Phys*., 45 6496-6500(2006)

[11] G. Haïat, F. Padilla, F. Peyrin, and P. Laugier: "Variation of ultrasonic parameters with microstructure and material properties of trabecular bone: a 3d model simulation," *J. Bone Miner. Res.,* 22, 665-674 (2007)

[12] Y. Nagatani, H. Imaizumi, T. Fukuda, M. Matsukawa, Y. Watanabe and T. Otani, "Applicability of Finite-Difference Time-Domain Method to Simulation of Wave Propagation in Cancellous Bone," *Jpn. J. Appl. Phys.,* 45 7186-7190 (2006)

[13] Y. Nagatani, K. Mizuno, T. Saeki, M. Matsukawa, T. Sakaguchi, H. Hosoi, “Numerical and Experimental Study on the Wave Attenuation in Bone -FDTD Simulation of Ultrasound Propagation in Cancellous Bone -”, *Ultrasonics*, Accepted.

[14] K. Mizuno, M. Matsukawa, T. Otani, M. Takada, I. Mano, T. Tsujimoto, “Effects of structural anisotropy of cancellous bone on speed of ultrasonic fast waves in the bovine femur.”, *Trans., IEEE., UFFC.,* in Press.

[15] Y. Yamato, M. Matsukawa, K. Yamazaki, H. Mizukawa, T. Yanagitani and A. Nagano, "Effects of hydroxyapatite crystallites orientation on ultrasonic wave velocities in bovine cortical bone," *Calcif. Tissue Int.* , 82, 162-169 (2008)